Original Article

Effects of thermal properties on weld pool geometry predictions and HAZ thermal cycles in SAW simulations of API 5L X80 steel heavy plates

Victor Tomassoni de Paiva Reis [1]
Geovane de Assis Faria [2,3]
Daynara Faustina Moreira de Oliveira [2,3]
Geraldo Lúcio de Faria [1]
Rodrigo Rangel Porcaro [1]*

Abstract

The effects of thermal properties adopted in numerical simulations of submerged arc welding (SAW) on the prediction of the geometry of the fusion zone (FZ) and the thermal cycles in the heat-affected zone (HAZ) were investigated for thick plates of API 5L X80 steel. Seven test cases were considered, using different approaches for defining thermal properties, including constant values, temperature-dependent properties (based on literature), and artificially increased thermal conductivity above the melting temperature. The simulation results were compared with experimentally obtained macrographs. Thermal properties significantly affected the geometric parameters of the FZ, particularly the fused area and the weld pool length on the surface. The heating rate up to 1300 °C was highly sensitive to the selected thermal properties, whereas the cooling rate in the critical 800–500 °C range showed comparatively limited variation among the cases. Although simplified thermal models exhibited reduced accuracy in predicting FZ geometry, they provided a consistent representation of HAZ thermal cycles while reducing computational time by up to 45%. Therefore, when the primary objective of the numerical simulation is to provide thermal cycles for subsequent physical simulations of the HAZ, the use of simplified thermal properties can be considered a technically sound and computationally efficient strategy.

Keywords: API 5L X80 steel; Numerical simulation; Physical simulation; Thermal modeling.

1 Introduction

Welding is a fundamental technology for countless industrial sectors, involving the interaction of complex thermal, mechanical, and metallurgical phenomena that ultimately govern microstructural formation, residual stress development, potential discontinuities, and, consequently, the mechanical behavior of steels [1–4].

For ferritic steels, the Heat Affected Zone (HAZ) shows a complex subdivision into distinct regions, primarily defined by the peak temperature attained, dwell time at critical temperatures, and local cooling rates [5]. Given that these HAZ sub-regions are generally quite narrow in real welds, thermomechanical simulators are commonly employed to evaluate, in a controlled and isolated manner, the effects of thermal cycles on each of these areas. This approach enables analyses with higher accuracy and adequate experimental repeatability [4,6,7]. In general, the simulation focuses on the grain growth region, with peak temperatures around 1300 °C or higher, and the intercritically reheated grain growth region, with maximum temperature around 900 °C or lower [3,4]. Occasionally, other peak temperatures may be of interest depending on the material or specific studies [5].

To ensure the representativeness of these physical simulations, it is essential to obtain or estimate, with the highest accuracy, the key-parameters of the thermal cycles experienced at each point of interest in the welded joint. While such data can be experimentally obtained or estimated, it is more convenient and economic to employ simplified analytical models or empirical models to calculate the parameters of interest [7-9].

Numerical simulations, based on Finite Element Method (FEM), is another approach used to evaluate thermal cycles. With technological advancements, dedicated computational programs for such simulations have been developed. Examples include ANSYS, ABAQUS, SysWeld, and SimufactWeld. These tools allow the simulation of welding processes by defining the heat source, processing parameters, material characteristics and properties, as well as joint geometry. After the simulation, it is possible to extract complete thermal

[1]*Departamento de Engenharia Metalúrgica e de Materiais - DEMET, Universidade Federal de Ouro Preto - UFOP, Ouro Preto, MG, Brasil.*
[2]*REDEMAT - Rede Temática em Engenharia de Materiais, Universidade Federal de Ouro Preto - UFOP, Ouro Preto, MG, Brasil.*
[3]*Universidade do Estado de Minas Gerais – UEMG,* Belo Horizonte, *MG, Brasil.*

**Corresponding author: rodrigo.porcaro@ufop.edu.br*
E-mails: victor.tomassoni@aluno.ufop.edu.br; geovane.faria@aluno.ufop.edu.br;daynara.oliveira@aluno.ufop.edu.br; geraldofaria@ufop.edu.br

cycle data from different points or nodes of interest, which can then be reproduced experimentally [4,6,10-12].

FEM simulations have already been established as effective tools for modeling different welding processes. However, as computational capabilities evolve, allowing increasingly complex models, the accuracy of results critically depends on the quality of input data and the precise definition of boundary conditions. As highlighted by Asserin et al. [13], one of the main challenges in thermal simulations concerns obtaining thermophysical and thermomechanical properties of materials dependent on the temperature, since these data require high-cost experimental methods and advanced technical procedures. Furthermore, for certain specific materials, data available in the literature is either scarce or does not cover the entire temperature range and relevant properties necessary for accurate simulation of the welding process [10,13].

In this context, the present study evaluated the effects of variations in thermophysical properties on the welding pool geometry and thermal cycles in two HAZ regions. Numerical simulations using FEM were performed for the Submerged Arc Welding (SAW) process on thick plates of API 5L X80 steel alloy – 25 mm. For this purpose, welding tests were performed under controlled conditions, in order to calibrate the heat source parameters and validate the numerical results regarding the fusion zone shape and the thermal profile.

This approach aims to contribute to the improvement of thermal modeling for arc welding processes, with the objective of obtaining key parameters for the physical simulation of HAZ sub-regions.

2 Development

2.1 SAW experiments

In order to obtain the geometric parameters of the heat source required for the numerical simulations, weld beads were deposited using the SAW process on a low-carbon steel plate with dimensions of 400 mm x 400 mm x 25 mm (length, width, and thickness, respectively), as illustrated in Figure 1. The welding conditions adopted were the same as those reported in [14], as presented in Table 1.

After deposition, the geometric parameters of the FZ were measured on the bead surface. Macrographs of the cross

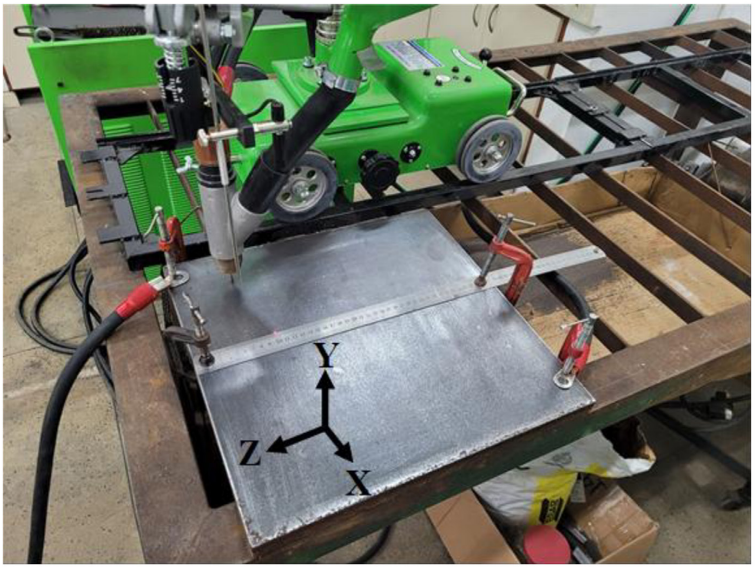

Figure 1. Experimental setup for weld bead deposition using the SAW process on thick steel plate. The base material was a low carbon steel (ASTM A36) with 400mm x 400mm x 25mm.

Table 1. Welding parameters and materials employed in the SAW depositions

Deposition Parameters			
Current (A)	***Voltage (V)***	***Welding speed (mm/s)***	T_0 **(°C)**
650	30	9.0	25
Materials			
Base Metal	***Wire-Electrode***		***Flux***
ASTM A36	AWS A5.17 EL12-4 mm		OK Flux 429

section were prepared following the standard procedures recommended by ASTM E3 [15] and analyzed using ImageJ for comparison with the numerical model results. The cross sections were extracted at the bead center in order to avoid transient regions at the beginning and end of the bead.

2.2 Numerical simulations by FEM

The welding thermal cycles by the SAW process were numerically simulated by FEM using Ansys®. All simulations focused on the temperature evolution in the grain growth zone (peak temperature of 1300 °C) and in the grain refining zone (peak temperature of 900 °C), evaluating the effects of variations in the adopted material properties.

The model is presented in Figure 2a, whose dimensions were 250 mm x 500 mm x 25 mm (length, width, and thickness, respectively). The dimensions were adequate to avoid edge effects and heat accumulation within the domain [12]. Similar as realized by Abreu et al. [1], the model was divided into three parts to facilitate the finite element mesh refinement. After the study of the mesh refinement, by the convergence of maximus temperatures values (variation under 5%, with the raise of the nodes number) [16], the model adopted had refinement equal to 2,0 mm on the central region – corresponding to the expected FZ and entire HAZ – and 15 mm in the outer regions. The extent of the refined region was defined to ensure that both the complete FZ and the full HAZ remained entirely within the 2.0 mm mesh domain in all simulated cases. The final model consisted of 49,906 elements and 219,544 nodes.

Thermal simulation was used to have the temperature variation (thermal cycle) in each node of the model, by a volumetric heat source on the plate [17, 18]. To answer this thermal problem in the time domain, non-linear analyses by finite elements were done, through the Transient Thermal module from Ansys® software, adopting the finite element 'HEX 20' (Parabolic Hexahedron) [19]. This approach was adopted in all simulated cases.

Goldak's et al. [18] double ellipsoid model was used (Equations 1 and 2) to simulate the heat source (for the reference system of Figure 2b) [17]. For that, the geometric parameters obtained from experimental deposits discussed in the last section were considered. To use Goldak's et al. model [18] at Ansys, a programming script in its own language (APDL) was created [20].

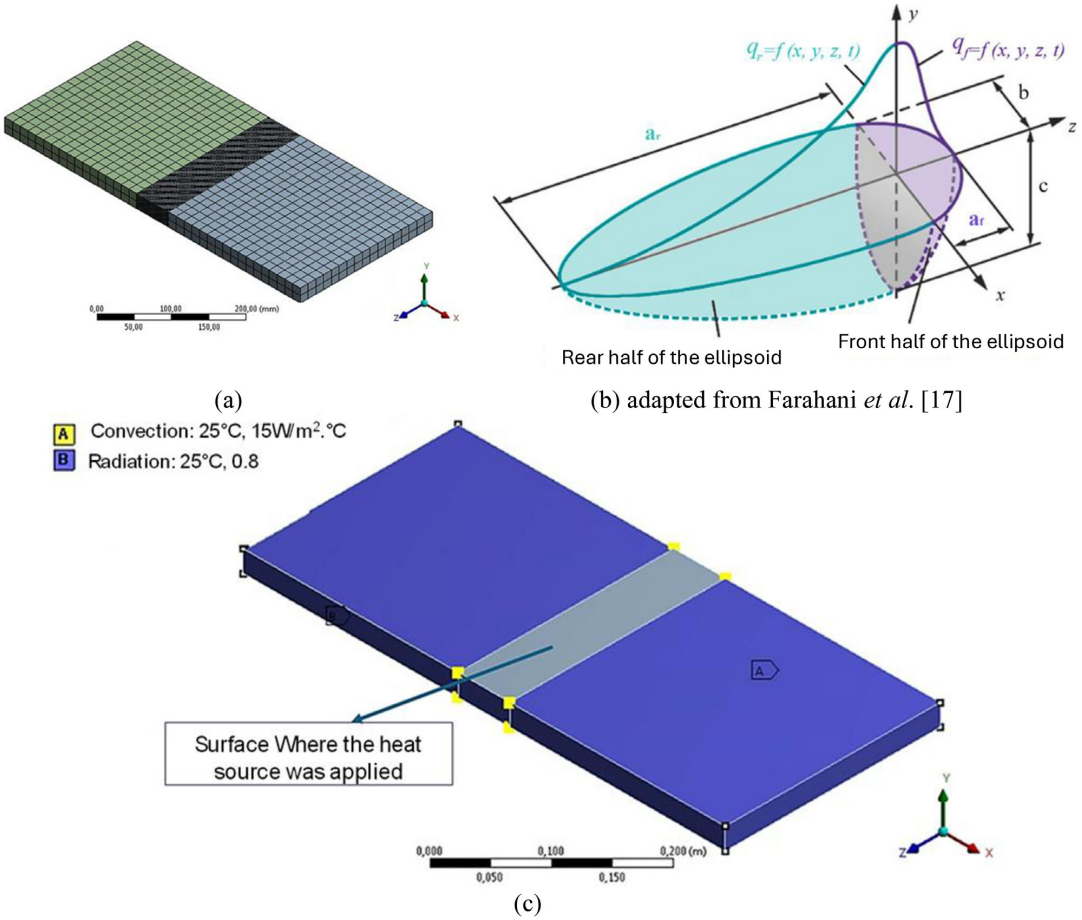

Figure 2. (a) Finite element mesh model adopted for thermal simulations of the SAW welding process. (b) Coordinate system and geometric parameters of the double-ellipsoid heat source model by Goldak et al. [18], the geometric parameters and the heat distribution are related to Equations 1 and 2. (c) Boundary conditions on the model surfaces: heat source, convection and radiation.

$$q_{,f} = F_f \frac{6\sqrt{3}Q}{a_f bc\pi^{3/2}} e^{-3\left[\left(\frac{z+v(t)}{a_f}\right)^2+\left(\frac{y}{c}\right)^2+\left(\frac{x}{b}\right)^2\right]} \quad (1)$$

$$q_{,r} = F_r \frac{6\sqrt{3}Q}{a_r bc\pi^{3/2}} e^{-3\left[\left(\frac{z+v(t)}{a_r}\right)^2+\left(\frac{y}{c}\right)^2+\left(\frac{x}{b}\right)^2\right]} \quad (2)$$

Where Q - effective power of the heat source (for the arc, Q=η·I·V) (W); t - time (s); v - travel speed of the heat source (welding speed, mm/s); x, y, and z, Cartesian coordinates of the model (Figure 2(b)). Ff and Fr - coefficients that determine the distribution of the heat between the front and rear portions of the ellipsoid, related to qf and qr; af, ar, b and c are four variables that define the semi-axes of the ellipsoid (mm). af corresponds to the front quadrant, ar to the rear quadrant, b is related to half the width, and c to the depth (penetration). The relationship between Ff e Fr is given by Equation 3, considering the continuity of the heat source [21]:

$$F_f = \frac{2a_f}{a_{f+a_r}}; F_f + F_r = 2 \quad (3)$$

The model also considered convection and radiation on the surfaces as boundary conditions, except for the heat source surface (Figure 2c). A convection coefficient of 15 W/m²°C, an ambient temperature of 25 °C, and an emissivity of 0.8 were considered [1].

The main objective of this study was to evaluate the effects of variations in the thermal properties of the materials (thermal conductivity and specific heat) on the thermal cycle results—focusing on the application of these data in physical simulations [9,11]—and on the geometry of the FZ. To this end, different temperature-dependent properties and strategies, as presented in Table 2, were simulated.

The temperature-dependent thermal properties for the seven cases are presented in Figure 3. The data used in cases 1 and 4 were extracted from the studies by Chunyan et al. [22] and Wang et al. [23], respectively, both of which addressed thermal simulations of API 5L X80 steel.

Despite referring to the same material specification, significant differences are observed between the models adopted by these authors, particularly regarding thermal conductivity and specific heat across the temperature range.

Case 5 aimed to evaluate the effects of using thermal properties provided by other authors [24], who performed simulations with low carbon steels. Cases 6 and 7 were

Table 2. Different numerical simulation strategies using FEM employed in this study

Simulated case	Source of the material properties	Strategy to compensate for the non-convection in the molten pool (FZ)
1	Chunyan et al. [22]	-
2	Chunyan et al. [22]	Increase in the thermal conductivity coefficient to 120 W/m·°C above the melting temperature
3	Chunyan et al. [22]	Increase in the thermal conductivity coefficient to 200 W/m·°C above the melting temperature
4	Wang et al. [23]	-
5	Deng and Murakawa [24]	Increase in the thermal conductivity coefficient to 120 W/m·°C above the melting temperature
6	Fu et al. [25] and Nguyen et al. [26]	-
7	Ansys [19]	-

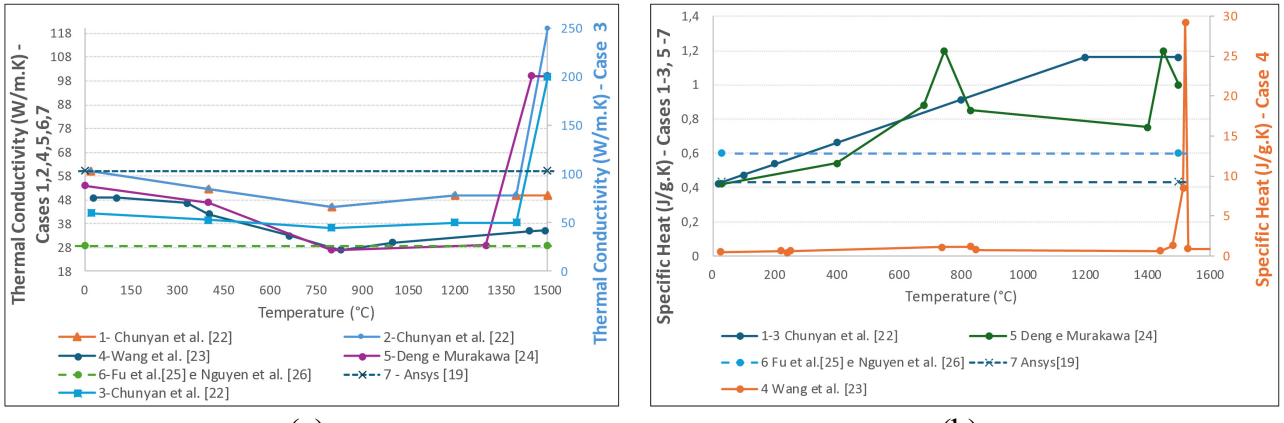

(a) (b)

Figure 3. Material models used for the SAW welding simulations and their respective comparative cases. (a) Thermal conductivity as a function of temperature. (b) Specific heat as a function of temperature. For Case 6, both thermal conductivity and specific heat were constant [25,26], with values of 29 W/m.K and 0.6 J/g.K, respectively. For Case 7, the values were also constant, at 60 W/m.K and 0.434 J/g.K, corresponding to the "Structural Steel" material in Ansys [19].

developed to investigate the impact of simplifying assumptions that disregard the variation of thermal conductivity and specific heat with temperature. In these two simulations, the values of these properties were kept constant from room temperature up to the melting point, using data extracted from references [25,26] and [19], respectively. It is important to note that the constant thermal property values reported in these references differ substantially from each other (Figure 3), particularly in terms of thermal conductivity, allowing the sensitivity of the numerical results to the magnitude of the adopted constant properties to be assessed. In all cases, density was assumed constant and equal to $\rho = 7870\ kg/m^3$ [1,10].

Numerical simulations of arc welding processes based on FEM generally do not consider convective effects in the weld pool [1,18,27]. To compensate for this limitation (which can lead to overestimation of peak temperature and inaccuracies in predicting weld bead geometry) several authors have adopted the strategy of artificially increasing thermal conductivity above the melting temperature [1,18,27]. In the present study, the impact of this approach was evaluated by comparing Cases 1, 2, and 3, which considered, respectively: (i) temperature-dependent thermal conductivity without adjustments; (ii) an increase to 120 W/m·°C; and (iii) an increase to 200 W/m·°C, both applied above the melting point (1500 °C), as indicated in Table 1 and Figure 3.

3 Results

3.1 SAW beads deposition

Figure 4a and b show the main results obtained from the bead-on-plate deposition experiments on thick plates using the SAW process, with the operational parameters described in Figure 1b.

Based on the results, the dimensions required to define the heat source Goldak's double ellipsoid heat source [18] were determined (Figure 2b) for reference) and Figure 4b). The parameters obtained were: af = 15.7 mm (frontal semi-axis), ar = 47.2 mm (rear semi-axis), b = 10.1 mm (half the width) and c = 6.8 mm (source depth).

Trupiano et al. [28] highlighted that the ideal definition of the geometric parameters of the heat source is one of the principal challenges in the arc weld simulation by Goldak's double ellipsoid model. These parameters directly influence the weld pool geometry, heat distribution and, consequently, the accuracy of the simulation results [25].

Under this difficulty of precisely defining these values, some authors used simplifications based on geometric proportions to reduce the number of variables to be determined.

For example, Fut et al. [25] adopted ar = 4af and b = af, while Nart and Celik [29] used b = c and ar = 3af. Li et al. [30] adopted af = 1/2c and ar = 2c, however, the authors discussed that obtaining real joints would be the best approach to find the dimensions.

In this study, the geometric parameters experimentally obtained were used to define Goldak's heat source model [18], as illustrated in Figure 2b and described in Equations 1 and 2. Moreover, using Equation 3, it was experimentally obtained Ff = 0.5, resulting in Fr = 1.5.

3.2 Numerical simulations

The results of the numerical simulations of SAW welding and their comparison with experimental data are shown in Figures 5b-h. A representative numerical result is presented in Figure 5a, which illustrates the temperature distribution generated by the heat source from Case 1, through the YZ and YX cutting planes.

Figures 5b-h present a comparison between the FZ obtained in the numerical simulations and the macrographs of

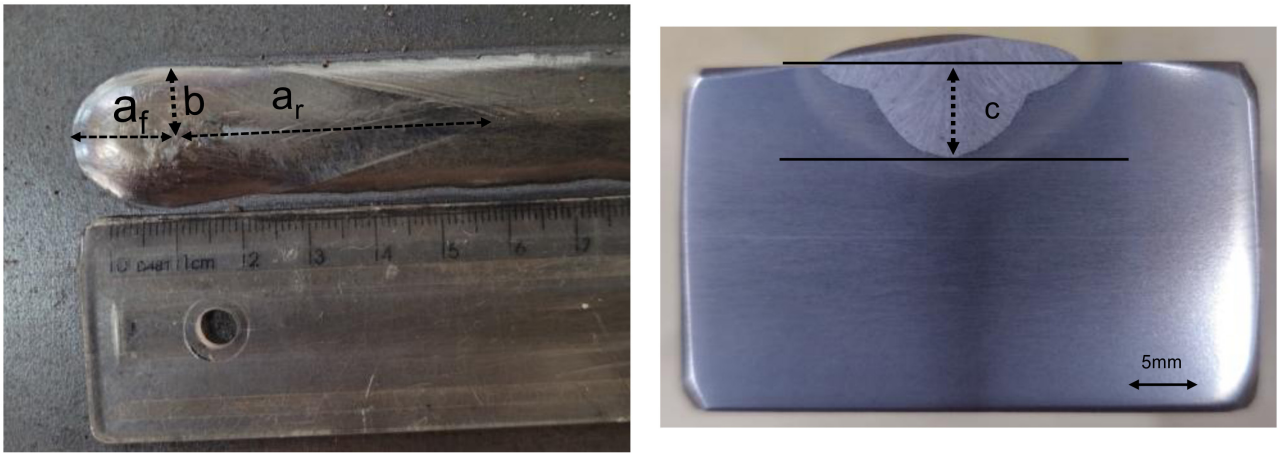

Figure 4. Results of bead-on-plate welds on thick plate using the SAW process. (a) Photograph of the weld pool showing the measurements of the front semi-axis (af), rear semi-axis (ar), and transverse semi-axis (b). (b) Macrograph of a transverse cross-section at the center of the weld bead indicating the source depth.

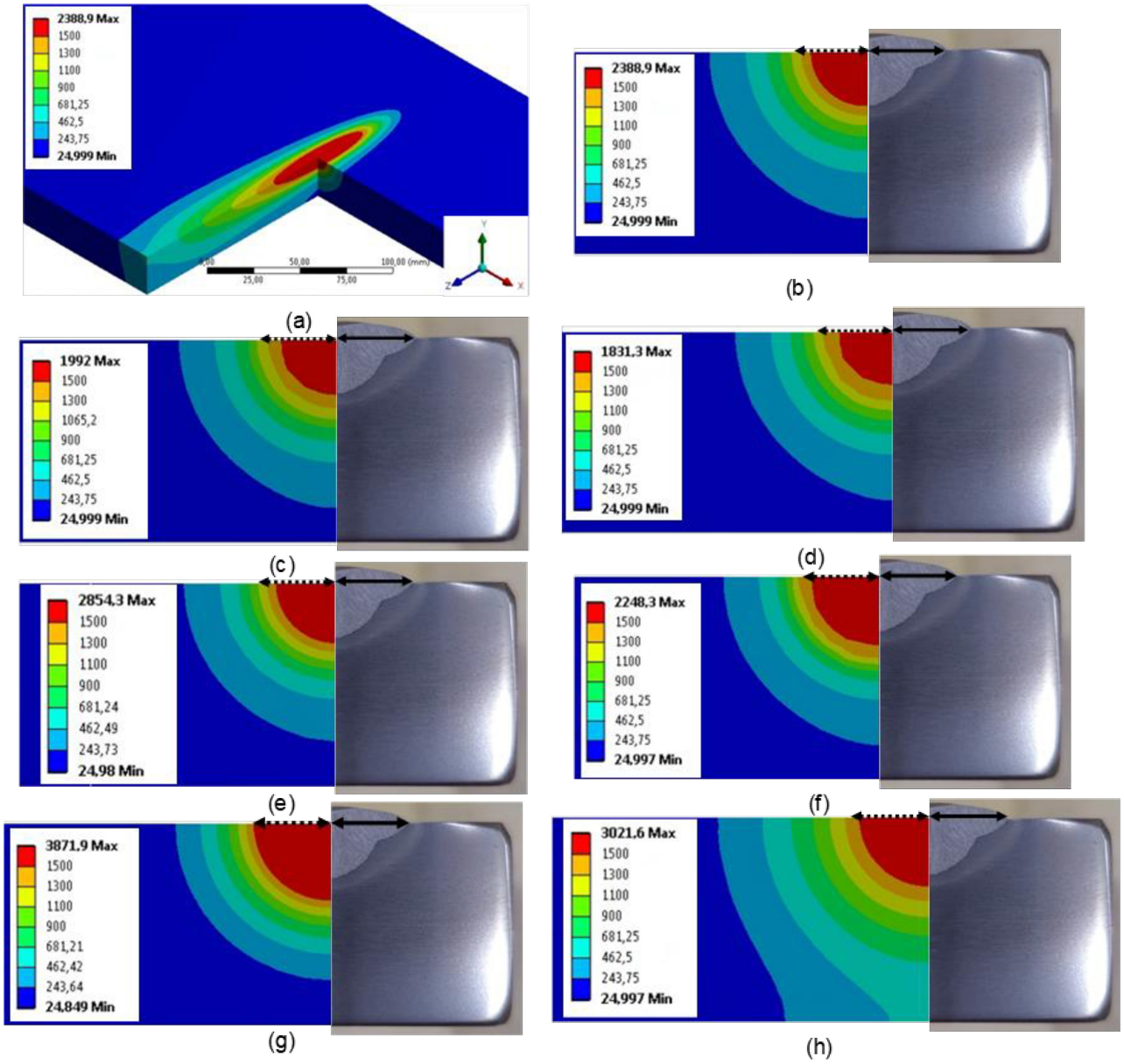

Figure 5. Results of numerical simulations of SAW welding and comparison with experimental data. (a) Overview of the transient temperature distribution during the heat source movement in Case 1. (b), (c), (d), (e), (f), (g), (h) comparison between numerical model results from Cases 1, 2, 3, 4, 5, 6, and 7, respectively, and the macrograph of the experimentally obtained transverse cross-section.

the experimentally produced welds. The geometric parameters of the simulated FZ were extracted using ImageJ software and are presented in Table 3.

Although the numerical model does not account for material deposition and, consequently, for the weld reinforcement, it can be observed that the global geometric parameters of the FZ (such as fused area and penetration depth) show good agreement with the experimental measurements.

In Figure 5, the melting temperature of the material was assumed to be 1500 °C, as suggested by Wang et al. [23].

Despite the overall agreement in global geometric parameters, differences in the weld pool morphology are observed when comparing the simulated FZ with the experimental macrographs, particularly regarding the characteristic "finger-shaped" profile commonly reported for SAW welds. This type of discrepancy has been widely discussed in the literature, and several studies have proposed alternative heat source models to improve the prediction of weld pool shape [23,27]. However, when the objective of the simulation is to obtain thermal cycles in the HAZ, the influence of the heat source model on the predicted thermal history has been shown to be limited [1].

An analysis of Cases 1, 2, and 3 (Figures 5b, 5c, and 5d, respectively) shows that the artificial increase in thermal conductivity above the melting temperature led to a substantial reduction in the maximum simulated temperature,

decreasing from 2388 °C in Case 1 to 1831 °C in Case 3. In contrast, as indicated in Table 2, the increase in thermal conductivity considerably reduced the length of the fusion zone at the model surface, demonstrating that this approach predominantly affects the longitudinal extension of the weld pool rather than its transverse dimensions. Similar findings were reported by Podder et al. [27], who simulated SAW welding of a low-carbon steel and observed that artificially increasing the thermal conductivity from 31.3 W/m·°C to 259.3 W/m·°C was necessary to limit excessive peak temperatures in the molten pool without underestimating peak temperatures in the HAZ.

The data presented in Table 3 demonstrate that the thermal properties adopted in the simulations have a significant influence on the geometric parameters of the fusion zone (FZ). As previously discussed, the original double ellipsoid model [18] has shown limitations in predicting FZ geometry in weld simulations performed using the SAW process [23,27]. It is also important to note that the simulations presented here did not account for weld reinforcement or material deposition, which may further affect the predicted weld bead profile. Considering exclusively the geometric agreement between the simulated and experimental FZ cross-sections, Cases 5 and 7 exhibited the closest correspondence to the measured dimensions. Notably, although Case 7 employed constant thermal properties over the entire temperature range, it yielded FZ geometric parameters comparable to the experimental values while reducing the simulation time by approximately 45% relative to Case 5.

Figure 6a presents the thermal cycles obtained for the seven simulated cases, considering 1300 °C as peak temperature (coarse-grained HAZ). Table 4 summarizes the effects of varying thermal properties in the simulations on the main parameters of the thermal cycles in the two evaluated regions of the HAZ (1300 °C and 900 °C–fine -grained HAZ).

Experimental data for cooling rates were estimated using simplified analytical models, as described by Li *et al.* [30] and according to EN 1011-2 [31,32]. Table 4 shows that the

Table 3. Results of the geometric parameters of the fusion zone obtained by simulation in comparison with experimental data

Evaluated case	Simulation time (min)	Fusion Zone Parameters and Their Respective Errors (difference between simulated and experimental values)*							
		Fused area		Penetration (Depth)		Width on the surface		Length on the surface	
		(mm^2)	Error (%)	(mm)	Error (%)	(mm)	Error (%)	(mm)	Error (%)
Experimental	-	**101**	-	**6.8**	-	**20.2**	-	**63**	-
1	131	66	-35	6.8	0	13.4	-34	66	5
2	138	73	-28	6.8	0	13.5	-33	55	-13
3	154	71	-30	6.7	-1	13.5	-33	49	-22
4	162	84	-17	7.4	9	14.8	-27	111	76
5	157	113	12	8.4	24	16.8	-17	67	6
6	91	138	37	9.5	40	19.0	-6	105	67
7	87	108	7	8.6	26	16.7	-17	65	3

*Error calculated as: Error = [(simulated parameter – experimental parameter) / experimental parameter] × 100.

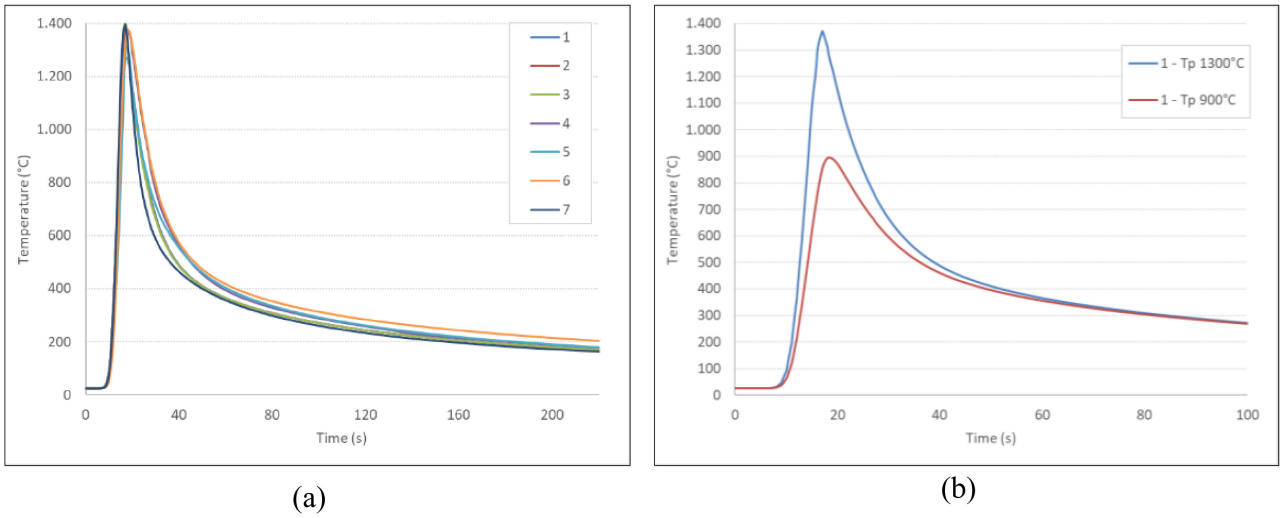

Figure 6. (a) Results of numerical simulations of the SAW welding process: thermal cycles obtained for the 7 simulated cases considering a peak temperature (PT) of 1300 °C. (b) Comparison between thermal cycles for PT equal to 1300 °C and 900 °C from case 1 obtained through simulation.

Table 4. Effects of material properties (simulated cases) on the results of thermal cycles obtained by simulation of SAW welding in comparison to calculated values.

Simulated cases	Peak Temperature 1300 °C			Peak Temperature 900 °C	
	Heating (°C/s)	Cooling (°C/s)		Heating (°C/s)	Cooling (°C/s)
	25-1300 (°C)	1300-800 (°C)	800-500 (°C)	25-900 (°C)	800-500 (°C)
1	**112**	**56**	**24**	**91**	**23**
2	129	61	24	83	22
3	133	61	24	85	22
4	132	54	19	67	17
5	126	57	17	78	16
6	130	52	18	75	18
7	148	93	24	87	25
Calculated	-	-	24[1]	-	-
	-	-	27[2]	-	-

[1] – Analytical models [30] with thermal conductivity of 29 W/m.K [26]. [2] – Empirical equations [31,32] considering thick plates.

choice of thermal properties has a significant impact on the simulated thermal cycle parameters. It is observed that the heating rate—for both the region with a peak temperature of 1300 °C (grain growth) and peak temperature of 900 °C (grain refinement)—varied considerably among the evaluated cases. This reflects the strong influence of the adopted thermal properties. In contrast, the cooling rate within the critical range of 800–500°C exhibited lower sensitivity, with values ranging from 16 °C/s to 25 °C/s, which are relatively close to those estimated by simplified analytical models (24–27 °C/s) [31-33].

Overall, the cases that most closely approximated the reference values for the 800–500 °C cooling rate—particularly Cases 1, 2, 3, and 7—were the most suitable for applications in physical simulation of the HAZ. Among them, Case 7 is particularly noteworthy, as it achieved results consistent with the analytical predictions while assuming constant thermal properties, reinforcing its suitability as a computationally efficient alternative when the primary objective is to reproduce HAZ thermal cycles.

Another observation is that, regardless of the peak temperature considered (1300 °C or 900 °C), the cooling rates within the critical 800–500 °C range tended to converge to similar values across cases, which aligns with the findings of Kou [2]. To illustrate this behavior, Figure 6(b) shows the thermal cycles corresponding to the two peak temperatures for Case 1. The peak temperatures occur at different times, and the curves converge to similar slopes during cooling below 800 °C. As discussed by Messler Jr. [34], the peak temperatures in different HAZ sub-regions decrease as the distance from the weld centerline increases, and they occur at progressively later times. This happens because, in HAZ sub-regions with lower peak temperatures, part of the heating results from heat transfer from the fusion zone (including latent heat of fusion and conduction through the solid).

Zhu and Chao [35] investigated the effects of considering or neglecting temperature-dependent thermomechanical properties on temperature fields and residual stresses/distortions in FEM-based simulations of an aluminum alloy. The authors concluded that, apart from yield strength, all other properties—including thermal conductivity, specific heat, and density—exerted negligible influence on temperature distribution and residual stress fields. In a similar study, Sepe et al. [36] evaluated the impact of accounting for temperature-dependent thermomechanical properties in welding simulations of a structural steel. The results showed that using constant thermal properties did not produce significant changes in temperature distribution and enabled a 60% reduction in simulation time. However, regarding residual stresses, the thermal expansion coefficient was highlighted as the most critical property and must be modeled as temperature-dependent to obtain more reliable results.

Lundin and Zhou [7] compared different methods available in thermomechanical welding simulators for obtaining thermal cycle parameters, focusing on physical simulation of arc welding. The authors noted that commercial and analytical models reported in the literature exhibited considerable discrepancies, particularly in predicting the cooling rate in the critical 800–500 °C range, with differences exceeding 150%.

The results obtained in this study can be used to define more rational strategies with lower computational cost and reduced simulation time, aiming to obtain complete thermal cycles for application in physical simulations of HAZ sub-regions. Although analytical or empirical models allow reasonably accurate estimation of cooling rates between critical temperatures—such as within the 800–500 °C range—numerical simulations provide greater accuracy in determining other relevant thermal cycle parameters, such as heating rates and dwell times above specific temperatures. This information is essential for conducting more representative physical simulations and for understanding metallurgical phenomena occurring in the HAZ, as discussed by Oliveira [37].

4 Conclusions

Based on the results obtained, it is concluded that the definition of thermal properties in numerical simulations of SAW welding plays a decisive role in predicting fusion zone

(FZ) geometry and selected thermal cycle parameters in the heat-affected zone (HAZ). The geometric characteristics of the FZ were particularly sensitive to the adopted thermal conductivity values, while the heating rate up to the peak temperature showed strong dependence on the thermal property model. The use of constant thermal properties proved to be a viable and efficient simplification, reducing simulation time by approximately 45% compared to temperature-dependent models. Although this approach presents limitations in accurately reproducing certain geometric features of the FZ, it maintained satisfactory agreement with experimental measurements and analytical cooling rate estimates in the critical 800–500 °C range. The artificial increase in thermal conductivity above the melting temperature effectively reduced the simulated peak temperature without significantly affecting FZ width or penetration depth, although it noticeably shortened the longitudinal extension of the weld pool at the model surface. Overall, the results demonstrate that, when the primary objective of the simulation is to generate reliable thermal cycles for subsequent physical simulation of the HAZ, a carefully designed simplification of the material model constitutes a technically sound and computationally efficient strategy, enabling substantial reduction in computational cost without compromising the accuracy required for HAZ-focused analyses.

Acknowledgements

This work was supported by the Brazilian Federal Agency (CAPES) – Funding Code 001, and by the Federal University of Ouro Preto (UFOP), where the experimental tests were conducted. The authors also acknowledge the financial support from FAPEMIG (Grant APQ-00245-23) and CNPq.

References

1 Abreu SGPT, Porcaro RR, Faria GL, Godefroid LB, Pereira IC, Souza SS. Austenitizing temperature effects on the martensitic transformation and its influence on simulated welding residual stresses in a microalloyed-steel. Materials Research. 2023;26:e20220624. https://doi.org/10.1590/1980-5373-MR-2022-0624.

2 Kou S. Welding metallurgy. 2nd ed. Hoboken, NJ: John Wiley & Sons; 2003.

3 Singh MP, Arora KS, Kumar R, Shukla DK, Siva Prasad S. Influence of heat input on microstructure and fracture toughness property in different zones of X80 pipeline steel weldments. Fatigue & Fracture of Engineering Materials & Structures. 2021;44(1):85-100. https://doi.org/10.1111/ffe.13333.

4 Payão JC Fo, Girão IF, Oliveira VHPM, Ramos IR. Estudo da zona afetada pelo calor de aço API 5L X100 com simulação computacional e física. In: Anais do 72° Congresso Anual da ABM; 2017; São Paulo, Brazil. São Paulo: ABM; 2017. p. 2594-5327.

5 Porcaro RR, Faria GL, Godefroid LB, Apolonio GR, Cândido LC, Pinto ES. microstructure and mechanical properties of a flash butt welded pearlitic rail. Journal of Materials Processing Technology. 2019;270:20-27. https://doi.org/10.1016/j.jmatprotec.2019.02.013.

6 Rios MCG, Payão JC Fo, Farias FWC, Oliveira VHPM, Passos AV. Microstructural characterization of the simulated heat-affected zone of 9 Pct Ni steel. Metallurgical and Materials Transactions. A, Physical Metallurgy and Materials Science. 2021;52(11):5016-5031. https://doi.org/10.1007/s11661-021-06446-8.

7 Lundin CD, Zhou G. A comparison of published HAZ thermal simulation methods used to derive weld HAZ thermal cycles. Acta Metallurgica Sinica. English Letters. 2000;13(1):223-232.

8 Cezário ALS, Porcaro RR, Faria GL. Proposição de um modelo empírico para determinação das temperaturas críticas durante resfriamento contínuo em zonas termicamente afetadas de aços IF soldados pelo processo TIG. Soldagem e Inspeção. 2019;24:1-14. https://doi.org/10.1590/0104-9224/si24.20.

9 Oliveira DFM, Porcaro RR, Faria GL. Simulação numérica e física do processo de soldagem ao arco submerso de um aço API 5L. In: In: Associação Brasileira de Metalurgia, Materiais e Mineração. Anais do 77° Congresso Anual da ABM – Internacional; 2024; São Paulo, Brazil. São Paulo: ABM; 2024. p. 1996-2010.

10 Nobrega J, Silva D, Araujo B, Melo R, Maciel T, Silva A, et al. Numerical evaluation of multipass welding temperature field in API 5L X80 steel welded joints. The International Journal of Multiphysics. 2014;8(3):337-348. https://doi.org/10.1260/1750-9548.8.3.337.

11 Dornelas PHG, Payão JC Fo, Oliveira VHPM, De Oliveira MD, Zumpano P Jr. Studying the nfluence of the interpass temperature on the heat-affected zone of an API 5L X65 steel welded pipe joint through computational and physical simulations. International Journal of Pressure Vessels and Piping. 2021;194(Pt b):104548.

12 Porcaro RR, Araújo FC, Godefroid LB, Faria GL, Silva LL. Simulação do Processo de Soldagem Elétrica por Centelhamento de um Aço para Trilhos Ferroviários. Parte 2: Análise Dilatométrica e Numérica. Soldagem e Inspeção. 2020;25:1-11. https://doi.org/10.1590/0104-9224/si25.33.

13 Asserin O, Loredo A, Petelet M, Looss B. Global sensitivity analysis in welding simulations–What are the material data you really need? Finite Elements in Analysis and Design. 2011;47(9):1004-1016. https://doi.org/10.1016/j.finel.2011.03.016.

14 Lan L, Kong X, Qiu C, Zhao D. Influence of microstructural aspects on impact toughness of multi-pass submerged arc welded HSLA steel joints. Materials & Design. 2016;90:488-498. https://doi.org/10.1016/j.matdes.2015.10.158.

15 American Society for Testing and Materials – ASTM. ASTM E3: standard guide for preparation of metallographic specimens. West Conshochen: ASTM; 2017.

16 Nezamdost MR, Esfahani MRN, Hashemi SH, Mirbozorgi SA. Investigation of temperature and residual stresses field of submerged arc welding by finite element method and experiments. International Journal of Advanced Manufacturing Technology. 2016;87(1-4):615-624. https://doi.org/10.1007/s00170-016-8509-4.

17 Farahani EB, Sarhadi A, Alizadeh-Sh M, Fæster S, Danielsen HK, Eder MA. Thermomechanical modeling and experimental study of a multi-layer cast iron repair welding for weld-induced crack prediction. Journal of Manufacturing Processes. 2023;104:443-459. https://doi.org/10.1016/j.jmapro.2023.08.059.

18 Goldak J, Chakravarti A, Bibby M. A new finite element model for welding heat sources. Metallurgical Transactions. B, Process Metallurgy. 1984;15(2):299-305. https://doi.org/10.1007/BF02667333.

19 Ansys Inc. Product launcher release 17.0. ANSYS17.0 help. Canonsburg: Ansys Inc; 2016.

20 Barban LM. Análise numérico-computacional das tensões térmicas induzidas pela soldagem [dissertação]. São Paulo: Engenharia Mecânica de Projeto e Fabricação, Universidade de São Paulo; 2014.

21 Lundbäck A. Finite element modelling and simulation of welding of aerospace components [thesis]. Luleå, Sweden: Department of Applied Physics and Mechanical Engineering Division of Computer Aided Design, Luleå Tekniska Universitet; 2003.

22 Chunyan Y, Cuiying L, Bo Y. 3D modeling of the hydrogen distribution in X80 pipeline steel welded joints. Computational Materials Science. 2014;83:158-163. https://doi.org/10.1016/j.commatsci.2013.11.007.

23 Wang ZW, Shang C, Wang X. Development of a finite element model for the HAZ temperature field in longitudinal welding of pipeline sttel. Metals. 2025;15:1-17.

24 Deng D, Murakawa H. Prediction of welding distortion and residual stress in a thin plate butt-welded joint. Computational Materials Science. 2008;43(2):353-365. https://doi.org/10.1016/j.commatsci.2007.12.006.

25 Fu G, Lourenço MI, Estefen MDSF. Parameter determination of double-ellipsoidal heat source model and its application in the multi-pass welding process. Ships and Offshore Structures. 2014;10(2):204-217.

26 Nguyen N, Ohta A, Matsuoka K, Suzuki N, Maeda Y. Analytical solutions for transient temperature of semi-infinite body subjected to 3D moving heat sources. Welding Journal. 1999;3:265s-274s.

27 Podder D, Mandal NR, Das S. Heat source modeling and analysis of submerged arc welding. Welding Journal. 2014;93:183s-192s.

28 Trupiano S, Belardi VG, Fanelli P, Gaetani L, Vivio F. A semi-analytical method for the calculation of double-ellipsoidal heat source parameters in welding simulation. IOP Conference Series: Materials Science and Engineering. 2022;1214:012023. https://doi.org/10.1088/1757-899X/1214/1/012023.

29 Nart E, Celik Y. A practical approach for simulating submerged arc welding process using FE method. Journal of Constructional Steel Research. 2013;84:62-71. https://doi.org/10.1016/j.jcsr.2013.02.005.

30 Li Y, Huang M, Lu X. Improvement in ovality of pipeline steel X80 with weld power under multi-wire SAW Welding Process. Advanced Materials Research. 2011;239-242:1823-1831. https://doi.org/10.4028/www.scientific.net/AMR.239-242.1823.

31 Marques PV, Modenesi PJ. Algumas equações úteis em soldagem. Soldagem e Inspeção. 2014;19(1):91-102. https://doi.org/10.1590/S0104-92242014000100011.

32 European Standards. BS EN 1011-2. 1-62. Welding – recommendations for welding of metallic materials – part 2: arc welding of ferritic steels. London: British Standard; 2001.

33 Rust B, Schmidt J, Stroetmann R. Influence of the cooling time $t_{8/5}$ on weld metals. Welding in the World. 2025;69(10):1-14. https://doi.org/10.1007/s40194-025-01942-6.

34 Messler JRW. Principles of welding: processes, physiscs, chemistry, and metallurgy. Weinheim: WILEY-VCH Verlag GmbH & Co. KgaA; 2004. 662 p.

35 Zhu XK, Chao YJ. Effects of temperature-dependent material properties on welding simulation. Computers & Structures. 2002;80(11):967-976. https://doi.org/10.1016/S0045-7949(02)00040-8.

36 Sepe R, Greco A, De Luca A, Caputo F, Berto F. Influence of thermo-mechanical material properties on the structural response of a welded butt-joint by FEM simulation and experimental tests. Forces in Mechanics. 2021;4:1-16. https://doi.org/10.1016/j.finmec.2021.100018.

37 Oliveira DFM. Efeitos dos parâmetros de soldagem SAW sobre a microestrutura da região de crescimento de grão reaquecida intercriticamente em um aço API 5L X80 - simulações numéricas e físicas [dissertação]. Ouro Preto: Escola de Minas, Universidade Federal de Ouro Preto; 2025.

Received: 21 Oct. 2025
Accepted: 01 Mar. 2026

Editor-in-charge:
André Luiz Vasconcellos da Costa e Silva